Nanoscale

PAPER

View Article Online
View Journal | View Issue

Cite this: *Nanoscale*, 2016, **8**, 1066

Two-dimensional material-based saturable absorbers: towards compact visible-wavelength all-fiber pulsed lasers†

Zhengqian Luo,‡[a] Duanduan Wu,‡[a] Bin Xu,[a] Huiying Xu,[a] Zhiping Cai,*[a] Jian Peng,[b] Jian Weng,*[b] Shuo Xu,[c] Chunhui Zhu,[c] Fengqiu Wang,*[c] Zhipei Sun[d] and Han Zhang[e]

Passive Q-switching or mode-locking by placing a saturable absorber inside the laser cavity is one of the most effective and popular techniques for pulse generation. However, most of the current saturable absorbers cannot work well in the visible spectral region, which seriously impedes the progress of passively Q-switched/mode-locked visible pulsed fibre lasers. Here, we report a kind of visible saturable absorber—two-dimensional transition-metal dichalcogenides (TMDs, *e.g.* WS_2, MoS_2, $MoSe_2$), and successfully demonstrate compact red-light Q-switched praseodymium (Pr^{3+})-doped all-fibre lasers. The passive Q-switching operation at 635 nm generates stable laser pulses with ~200 ns pulse duration, 28.7 nJ pulse energy and repetition rate from 232 to 512 kHz. This achievement is attributed to the ultrafast saturable absorption of these layered TMDs in the visible region, as well as the compact and all-fibre laser-cavity design by coating a dielectric mirror on the fibre end facet. This work may open a new route for next-generation high-performance pulsed laser sources in the visible (even ultraviolet) range.

Received 9th October 2015,
Accepted 26th November 2015

DOI: 10.1039/c5nr06981e

www.rsc.org/nanoscale

Introduction

Compact and efficient visible-wavelength pulsed lasers are of great interest for various applications, including underwater detection, laser medicine, and biomedical imaging. Although visible-wavelength pulsed solid-state bulk laser systems (*e.g.* Ti: sapphire pumped optical parametric oscillators) have been relatively matured, limitations in terms of footprint, cost and efficiency have called for alternative laser solutions. For some practical applications, it is highly desired that visible-wavelength pulsed sources are compact, user-friendly, low-cost and maintenance-free. Fortunately, visible pulsed all-fibre lasers could satisfy all these demands. At present, visible pulsed fibre sources are mainly based on frequency conversion techniques (*e.g.* fibre optical parametric oscillator[1] or supercontinuum generation[2,3] in photonic crystal fibres,[4] frequency doubling of near-infrared fibre lasers,[5] and up-conversion fibre lasers[6]). Although these techniques, by exciting optical nonlinear processes in fibres, can indeed convert infrared pumping light into widely-tuneable visible light,[1,2] they often suffer from low efficiency, instability or a complex structure. In contrast, if one combines rare-earth-doped fibre gain with Q-switching or mode-locking technologies, compact and efficient visible pulsed laser oscillators without additional frequency conversion methods could be expected and become more attractive. The main challenges for the past decades are from: (1) fabricating the low-loss visible gain fibres, (2) requiring high-power short-wavelength (ultraviolet or blue) pump laser diodes (LDs), and (3) obtaining a suitable visible-available Q-switch or mode-locker. Thanks to the fast development of soft-glass fibres (*e.g.* ZBLAN fibre) and high-power blue GaN LDs in recent years, exciting progress in continuous-wave visible Pr^{3+}-doped ZBLAN fibre lasers has been made,[7] but the pulsed operation of a visible fibre laser is very rare.[8] Although active Q-switching by an acousto-optic modulator has been recently reported in visible wavelengths,[8] it sacrifices the all-fibre structure and increases the system cost. In contrast, passive Q-switching or mode-locking could be preferred, and this is therefore stimulating research on new saturable-absorption materials for passively Q-switched/mode-locked visible fibre lasers.

[a]*Department of Electronic Engineering, Xiamen University, Xiamen 361005, China. E-mail: zpcai@xmu.edu.cn*
[b]*Department of Biomaterials, College of Materials, Xiamen University, Xiamen 361005, China. E-mail: jweng@xmu.edu.cn*
[c]*School of Electronic Science and Engineering, Collaborative Innovation Center of Advanced Microstructures, Nanjing University, Nanjing 210023, China. E-mail: fwang@nju.edu.cn*
[d]*Department of Micro- and Nanosciences, Aalto University, FI-02150 Espoo, Finland*
[e]*College of Optoelectronic Engineering, Shenzhen University, 518060, China*
†Electronic supplementary information (ESI) available. See DOI: 10.1039/c5nr06981e
‡These authors contributed equally to this work.

In recent years, photonics based on two-dimensional (2D) materials has been extensively studied,[9] and is opening up a new playground with unprecedented opportunities for novel optoelectronic applications.[10–14] In particular, it was found that 2D materials could exhibit strong optical saturable absorption because of their unique optical and electronic properties.[15] Current research in 2D material-based saturable absorbers (SAs) primarily focuses on graphene,[16–18] topological insulators,[19,20] transition-metal dichalcogenides (TMDs)[21,22] and black phosphorus.[23] They have been widely used to passively Q-switch or mode-lock lasers in a wide range from 800 nm to 3 μm,[15,24–28] but all of them are still limited in the infrared wavelength operation. Up to now, 2D material-based SAs for pulsed fibre lasers have not yet become available in the visible region.

Interestingly, layered TMDs (MX_2: M = W, Mo; X = S, Se) are considered the first type of existing 2D semiconductors with a direct bandgap in the visible frequency range,[29] and therefore strong saturable absorption at visible wavelengths could be expected in these materials. In this article, we found that the few-layer TMDs (*i.e.* WS_2, MoS_2, $MoSe_2$) are available for visible SAs with superior performance in the visible wavelength range (*i.e.* ~7% modulation depth and ~5 ps ultrafast relaxation time at 635 nm wavelength), well suited for pulse generation in the visible spectral range. Furthermore, we demonstrate for the first time visible-wavelength passively Q-switched all-fibre laser systems based on these few-layer TMDs. This approach represents a new paradigm in compact, low-cost and high-performance visible pulsed fibre laser sources for diverse applications, including underwater detection, laser medicine, biomedical imaging, and indoor optical communication.

Experimental section

Fabrication and characterization of few-layer TMDs

The few-layer WS_2 (MoS_2 or $MoSe_2$) was prepared by the liquid-phase exfoliation method[30] (see Methods): the bulk WS_2 was sonicated in *N*-2-methyl pyrrolidone (NMP) to produce a few-layer WS_2 suspension. The transmission electron microscopy (TEM) image (Fig. 1a) shows that the exfoliated WS_2 was indeed thin 2D flakes. Furthermore, the distance between the adjacent hexagonal lattice fringes in the high-resolution TEM (HRTEM) image was measured to be 0.27 nm (Fig. 1b), which was consistent with the lattice space of the (100) plane. The X-ray diffraction (XRD) pattern of the exfoliated WS_2 showed a high [002] orientation and some characteristic peaks disappeared compared to the bulk WS_2 (Fig. 1c), indicating that the bulk WS_2 had been successfully exfoliated down to a few layers. The two characteristic Raman peaks at 351 and 418 cm^{-1} of the bulk WS_2 (Fig. 1d), assigned to the E^1_{2g} and A^1_g modes, respectively, were red-shifted in the exfoliated WS_2. Furthermore, the thickness of the exfoliated WS_2 nanoflakes measured by atomic force microscopy (AFM) was ~2–4 nm (Fig. 1e, insert), confirming that the WS_2 nanoflakes were around 3–6 layers as the thickness of single-layer WS_2 is about 0.7 nm.[31] Moreover, the exfoliated WS_2 dispersion showed several distinct but well-defined absorption peaks[32] (*e.g.* 635 nm, matching perfectly with our laser operation wavelength) in the visible region (Fig. 1f). All the results indicate that high-quality few-layer WS_2 has been successfully prepared. Few-layer MoS_2 and $MoSe_2$ were also prepared by using a similar liquid-phase exfoliation method (ESI†).

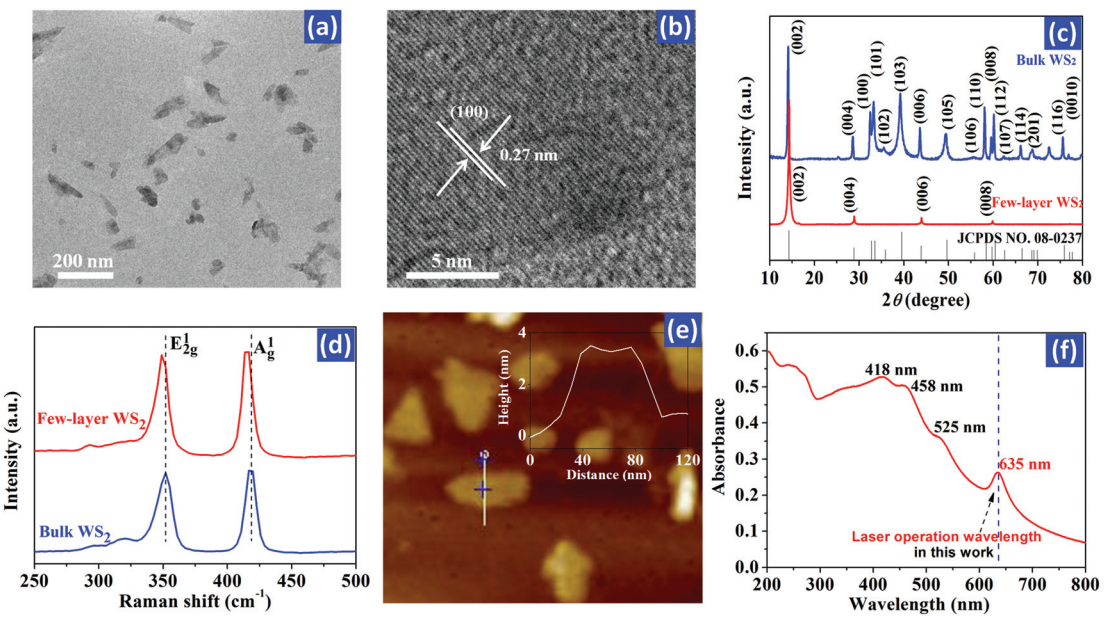

Fig. 1 Characterization of few-layer WS_2. (a) TEM image. (b) HRTEM image. (c) XRD patterns of the bulk WS_2 and few-layer WS_2. (d) Raman spectra of the bulk WS_2 and few-layer WS_2. (e) AFM image. Insert: the corresponding height profile of the few-layer WS_2 along the white line. (f) UV-vis absorption spectrum of the few-layer WS_2. The laser operation wavelength is shown as a dashed blue line.

Nonlinear optical properties of few-layer WS_2 at visible 635 nm wavelength

To investigate the saturable absorption properties of the few-layer TMDs in the visible wavelength, the open-aperture (OA) *Z*-scan technique (see Methods) was carried out at 635 nm, our red-light fibre laser operation wavelength. Nonlinear saturable absorption of all the as-prepared few-layer TDMs (WS_2, MoS_2, $MoSe_2$) could be observed in our experiment. Fig. 2a gives the representative results of the OA *Z*-scan traces for the few-layer WS_2 sample with the excitation powers of 1, 2.5 and 4 μW, respectively. The intensity-dependent transmittance of the few-layer WS_2 (*i.e.* as a function of position change) is clearly found, demonstrating the effective saturable absorption of the few-layer WS_2 at 635 nm. Note that the 635 nm wavelength is just located at one of the visible absorption peaks of the few-layer WS_2 (see Fig. 1f), and the resonant absorption is likely to enhance the saturable absorption at 635 nm. The slight asymmetry in the *Z*-scan traces is attributable to the inhomogeneity of the WS_2 sample, which was usually observed in the *Z*-scan measurements of layered materials.[33] Furthermore, pump–probe spectroscopy (see Methods) was also used to investigate the temporal dynamics of nonlinear optical properties of the few-layer TMDs. Using 635 nm degenerate pump/probe measurements, Fig. 2b shows the pump-induced change of probe transmission (ΔT) for the few-layer WS_2 sample with a pump fluence of ~1.5 mJ cm^{-2}. The response exhibits an initial photobleaching (PB) signal, and quickly turns into a photoinduced absorption (PA) one. The fast PB decay is about 5 ps, showing the ultrafast response of the few-layer WS_2 at the visible 635 nm wavelength. The emerging PA could be attributed to the surface defect trapped excitons, where the increasing occupation of defective states leads to a pronounced transition to higher energy levels.[34] In addition, we performed the same *Z*-scan measurement of the few-layer WS_2 at the 530 nm (green) wavelength, and a strong saturable absorption was also observed (see Fig. S3 in the ESI†). The PB relaxation process combined with the OA *Z*-scan results, nevertheless, confirms that the few-layer WS_2 exhibits ultrafast (~5 ps) saturable absorption with good performance (>7% modulation depth) in the visible range, very promising for pulse generation in the visible spectral range.

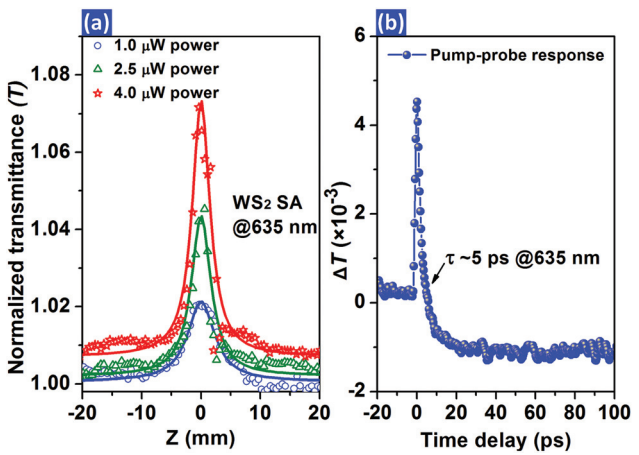

Fig. 2 Nonlinear optical properties of the few-layer WS_2 at 635 nm. (a) OA *Z*-scan traces with the excitation powers of 1, 2.5 and 4 μW, respectively. (b) Time-resolved differential transmission (ΔT) spectra with a pump fluence of ~1.5 mJ cm^{-2} using the 635 nm degenerate pump/probe.

Results and discussion

Experimental demonstration of TMD-based passively Q-switched visible fibre lasers

We further present the experimental demonstration of passively Q-switched visible fibre lasers based on few-layer WS_2, MoS_2 and $MoSe_2$, respectively. A photograph of this study is given in Fig. 3a, and the corresponding schematic of the experimental setup is shown in Fig. 3b. A piece of 98.5 cm Pr^{3+}-doped ZBLAN glass fibre (core/cladding: 6/125 μm, Pr^{3+} concentration: 1000 ppm) as a visible gain medium was pumped by a 445 nm/2 W GaN LD.[35] The end facets of the ZBLAN fibre were perpendicularly polished, and induced ~4% Fresnel reflection. The 445 nm pumping beam was firstly expanded by two optical lenses (L1 & L2) with different focal lengths, and then coupled into the core area of the ZBLAN fibre by a micro-objective lens (L3). The all-fibre based compact laser cavity for red-light oscillation was formed by the 4% Fresnel reflection of the ZBLAN fibre end-facet (left) and a fibre pigtail mirror M1 (right). The M1 was fabricated by directly coating multiple-layer dielectric films onto a fibre ferrule using a plasma sputter deposition system (see Methods). As seen in Fig. 3d, the dielectric films have been uniformly deposited on the fibre ferrule, and has a high transmittance of 97.2% at the pump wavelength of 445 nm as well as a high reflectivity of 99.8% at the wavelength range of 580–710 nm (*e.g.* T = 0.2%@635 nm, see Fig. 3e). Although the wide-waveband reflection of the M1 covers a few emission spectral peaks (see Fig. S4 in the ESI†) of the Pr^{3+}-doped ZBLAN fiber, the laser resonator could still operate only around 635 nm, because the gain competition always leads to the oscillation at the strongest gain peak (*i.e.* ~635 nm). In order to realize compact and stable visible-wavelength passive Q-switching, the key step is to compatibly insert the as-prepared few-layer TMDs into the laser cavity. A WS_2 polyvinyl alcohol (PVA) film [see Fig. 3c] was firstly fabricated by evaporating the WS_2/polymer composite solution to dryness, and was then sandwiched between the fibre pigtail mirror M1 and the Pr^{3+}-doped ZBLAN fibre end. The insertion loss of the WS_2/polymer SA film was measured to be 2.5 dB at 635 nm, and the damage threshold is estimated to be ~1.5 GW cm^{-2}. In addition, to conveniently couple out the laser, ~96% intracavity oscillating light was extracted, and then reflected by an angled dichroic mirror M2 (R > 99%@635 nm) as the laser output. The optical spectrum of the output laser was measured by using an optical spectrum analyzer, and the pulsed characteristics were detected by using a photodetector (PD) together

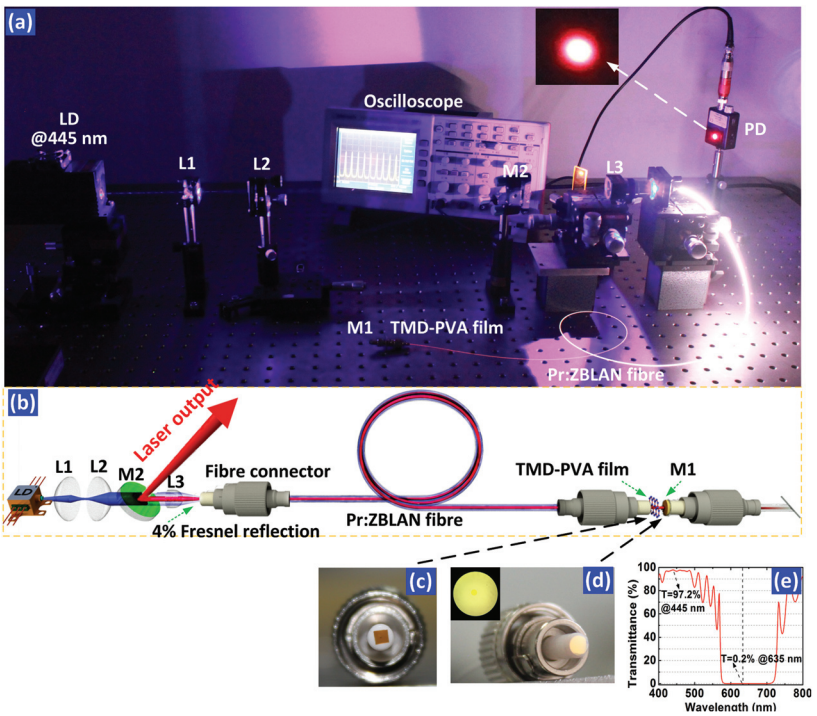

Fig. 3 Experimental setup and designs of the TMD-based passively Q-switched visible (red) fibre laser. (a) Photograph of the passively Q-switched visible fibre laser. Inset: the output beam spot. (b) Schematic of the visible fibre laser. (c) TMD-PVA film transferred to a ferrule of the fibre connector. (d) Highly-reflective dielectric films coated on a fibre ferrule (*i.e.* **M1**), inset: a close look at the dielectric film on the fibre end. (e) Optical transmission spectrum of the dielectric films. **L1**, **L2** and **L3**: lens. **PD**: photodetector.

with a digital oscilloscope and a radio-frequency (RF) spectrum analyzer.

Laser pulse generation at 635 nm wavelength

To confirm the significance of the TMD-based SA for passive Q-switching, we compare the laser output characteristics with and without the TMD-based SA in the cavity. Without using the TMD-based SA, it is confirmed that the 635 nm red laser always operated at the continuous-wave regime and no pulse train was observed. In contrast, once a TMD-based SA (*i.e.* WS_2-based SA) was placed inside the laser cavity, stable pulse trains self-started at the pump power of >143.6 mW. As shown in Fig. 4a, we measured the oscilloscope traces under different pump powers. With the increase of the pump power, the pulse repetition rate became larger and larger from 245.1 to 512.8 kHz while the pulse width became narrower. These phenomena are typical features of passive Q-switching,[22] and therefore verify that the WS_2-based SA plays an important role in the visible-wavelength passive Q-switching. At a pump power of 182.2 mW, we measured the typical output optical spectrum. As given in Fig. 4b, the lasing peak wavelength was located at 635.1 nm with a 3 dB linewidth of 0.08 nm. As shown in Fig. 4c, we also measured the RF output spectrum of the Q-switched pulse train. The fundamental RF peak f_0 (*i.e.* pulse repetition rate) is 353.0 kHz, and the RF signal-to-noise ratio (SNR) is as high as 43 dB (>10^4 contrast), indicating the good stability of the passive Q-switching operation. Furthermore, the broad-span RF output spectrum in the inset of Fig. 4c shows an RF envelope period of ~4 MHz, which is in good agreement with the measured pulse width of 244 ns in the temporal domain (according to the Fourier transform). As shown in Fig. 4d, we further recorded the pulse repetition rate and the pulse width of the visible passive Q-switching as a function of the incident pump power. The repetition rate can be widely tuned in the range of 232.7–512.8 kHz. The pulse width sharply decreased once the pump power was above the pump threshold, but remained almost unchanged when the pump power was over 180 mW. The minimum pulse width is 207 ns. In addition, the maximum average output power for the 635 nm passively Q-switched laser is 8.7 mW, and the maximum pulse energy is 28.7 nJ. In order to evaluate the output transverse-mode characteristics of the visible Q-switched fibre laser, we measured the optical intensity distribution using a laser beam analyzer (Spiricon LBA-400PC). As seen in Fig. 4e, the laser distribution from both the 2D and 3D photographs exhibits a good Gaussian shape, manifesting the single-transverse-mode operation of our fibre laser.

Moreover, we also achieved the 635 nm passively Q-switched Pr^{3+}-doped fibre lasers using few-layer MoS_2 and $MoSe_2$ (see Fig. S5 and S6 in the ESI†), respectively. Table 1 gives a summary of the performance of passive Q-switching using different TMD-based SAs (*i.e.* WS_2, MoS_2 and $MoSe_2$). It can be seen that their output parameters are very similar. The maximum output power (<10 mW) is relatively low, and could

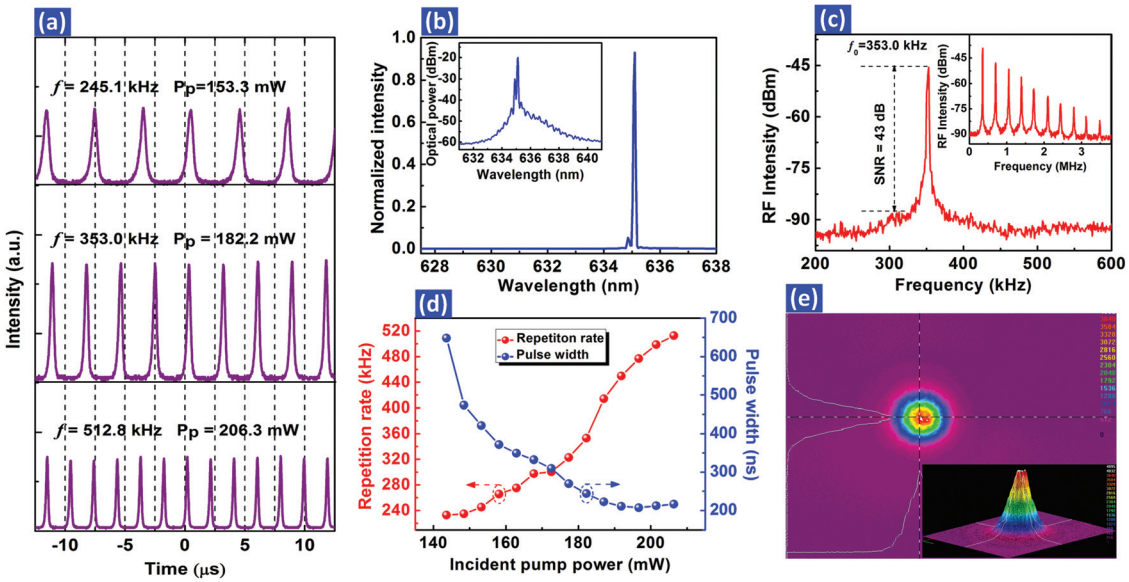

Fig. 4 Experimental results of the WS_2-based passively Q-switched visible (red) fibre laser. (a) Q-switched pulse trains under different pump powers. (b) Output optical spectrum of the Q-switching operation (inset: with a dBm logarithmic scale). (c) Typical RF output spectrum of the Q-switching operation (inset: the broad-span RF output spectrum). (d) Q-switched repetition rate and pulse width *vs.* the pump power. (e) Laser mode-field distribution.

Table 1 Performance of 635 nm passively Q-switched fiber lasers using three different TMD-based SAs

Materials (SAs)	Lasing wavelength (nm)	Q-switched threshold (mW)	Pulse duration (ns)	Repetition rate (kHz)	Max. output power (mW)
Few-layer WS_2	635.1	143.6	207	232.7–512.8	8.7
Few-layer MoS_2	635.5	148.4	227	240.4–438.6	7.1
Few-layer $MoSe_2$	635.4	146.8	240	357.1–555.1	6.2

be further improved by optimizing the output coupling ratio and increasing the pump coupling efficiency from the blue LD into the ZBLAN fiber core.

One could have concern about the fundamental mechanism of visible-wavelength saturable absorption in the few-layer WS_2, MoS_2 and $MoSe_2$. Since these layered TMDs have wide direct bandgaps[29] of ~2.0 eV (WS_2), ~1.9 eV (MoS_2) and ~1.5 eV ($MoSe_2$), respectively, their corresponding resonant wavelengths of ~620 nm (WS_2), ~690 nm (MoS_2) and ~800 nm ($MoSe_2$) are just located in or near the visible spectral region. Under the visible-light (*e.g.* 635 nm) illumination, electron–hole pairs from the layered TMDs can be in resonance (similar to carbon nanotubes[15]). This resonant process could make Pauli blocking very efficient, and contribute to the enhanced saturable absorption for nonlinear and ultrafast photonic applications in the visible operation wavelength.

Methods

Preparation of few-layer WS_2

The purchased bulk WS_2 (200 mg) was added into NMP (200 mL) and the solution was sonicated for 20 hours to produce the few-layer WS_2 suspension. The dispersion was then centrifuged at 2000 rpm for 30 min to remove bulk WS_2. Subsequently, the supernatant was decanted to another centrifuge tube. After centrifuging the supernatant at 13 000 rpm for 30 min to remove the free NMP, the as-obtained product was collected into vials for further characterization. Finally, we collected the few-layer WS_2 suspension into vials and dispersed it in polyvinyl PVA, which can be easily film-forming for further application.

Plasma sputter deposition for the fibre pigtail mirror

The plasma sputter deposition system (SCT-S500) is described in Fig. S7 in the ESI.† The plasma was initiated and amplified by a DC launch electromagnet towards the plasma source. The position of the plasma beam can be adjusted to ensure good beam impingement on the target surface. To achieve a high deposition rate in the reactive process, the RF power was adjusted from 1 to 2.2 kW and the target negative bias voltage was set from 300 to 700 V, respectively. During the deposition process, the system was pumped by a cryo-pump at a pressure of 6×10^{-6} Torr. Pure argon gas was introduced into the chamber, and the oxygen was fed into the chamber. The oxygen flow was regulated from 0 to 30 sccm with a fixed

argon flow of 85 sccm, and the background pressure is approximately 5×10^{-3} Torr. The fibre-based ferrules as the targets were used to deposit the dielectric films.

Z-Scan measurement

The *Z*-scan setup was based on a femtosecond optical parametric amplifier (OPA) which was pumped by a Ti:sapphire amplifier system (centre wavelength: 800 nm). Specifically, we have chosen an excitation wavelength of ~635 nm to study the nonlinear absorption of WS_2 samples in the visible range. The excitation pulse duration was ~100 fs (with a 1 kHz repetition rate) and a neutral density filter was employed to set the incident optical power. To avoid laser damage caused by either high peak intensity or thermal effects, we used our excitation power of <10 μW.

Pump–probe spectroscopy

For degenerate pump–probe experiments, the 635 nm femtosecond pulses were also from the OPA system used in the *Z*-scan. Here, the laser was split into pump and probe beams. The pump fluence is ~20 times larger than that of the probe fluence. Pump and probe beams had parallel polarization in our setup. The incident angle between the pump and probe beams was smaller than 15°. To record the small changes of the probe beam, the fluence of the probe was detected using a photo-detector and a lock-in amplifier referenced to a 500 Hz chopped pump.

Conclusions

We introduce 2D material-based SAs for all-fibre pulsed lasing in the visible regime. The red-light passive Q-switching generated stable pulse trains with a pulse width of ~200 ns and a wide range of repetition rates from 232.7 to 512.8 kHz. The present results suggest that the layered TMDs (WS_2, MoS_2 and $MoSe_2$) as visible SAs are extremely effective for generating short laser pulses in the visible regime. This could be mainly attributed to the wide bandgaps[30] (1.5–2.0 eV) of these TMDs to enhance the saturable absorption in the visible wavelength. In addition, by controlling the net dispersion of the Pr^{3+}-doped ZBLAN fiber laser and optimizing the cavity designs, such layered-TMD SAs may also enable passive mode-locking for generating ultrashort picosecond or femtosecond pulses in the visible wavelengths, and this will be the subject of our further work. In summary, this work has made a significant step towards the new-generation, compact, low-cost and high-performance pulsed fibre laser sources in visible (even ultraviolet) wavelengths.

Author contributions

Z. Q. Luo and Z. P. Cai conceived the original concept and designed the experiments. D. Wu and Z. Q. Luo performed the experiments on passively Q-switched Pr^{3+}-doped fibre lasers. J. Peng and J. Weng prepared and characterized the layered TMDs. S. Xu, C. Zhu and H. Zhang contributed to the *Z*-scan measurements. F. Q. Wang and Z. P. Sun performed pump–probe spectroscopy of the layered TMDs. B. Xu and H. Y. Xu contributed to the fibre pigtail mirror using the plasma sputter deposition system. All authors analyzed the experimental data. Z. Q. Luo, J. Weng, F. Q. Wang and Z. P. Sun co-wrote the paper. All authors discussed the results and revised the manuscript. Z. P. Cai and J. Weng advised on the project.

Acknowledgements

This work was supported by the National Nature Science Foundation of China (61275050, 61177044, 61475129, and 61378025) and by the National Key Scientific Research Projects (2014CB932004 and 2014CB921101) as well as the Specialized Research Fund for the Doctoral Program of Higher Education (20120121110034).

Notes and references

1 J. E. Sharping, M. A. Foster, A. L. Gaeta, J. Lasri, O. Lyngnes and K. Vogel, *Opt. Express*, 2007, **15**, 1474.
2 S. Coen, A. H. L. Chau, R. Leonhardt, J. D. Harvey, J. C. Knight, W. J. Wadsworth and P. S. J. Russell, *Opt. Lett.*, 2001, **26**, 1356.
3 J. Travers, S. Popov and J. R. Taylor, *Opt. Lett.*, 2005, **30**, 3132.
4 P. S. J. Russell, *Science*, 2003, **299**, 358.
5 L. R. Taylor, Y. Feng and D. B. Calia, *Opt. Express*, 2010, **18**, 8540.
6 D. S. Funk and J. G. Eden, *IEEE J. Sel. Top. Quantum Electron.*, 1995, **1**, 784.
7 H. Okamoto, K. Kasuga, I. Hara and Y. Kubota, *Opt. Express*, 2009, **17**, 20227.
8 J. Kojou, Y. Watanabe, P. Agrawal, T. Kamimura and F. Kannari, *Opt. Commun.*, 2013, **290**, 136.
9 A. K. Geim and K. S. Novoselov, *Nat. Mater.*, 2007, **6**, 183.
10 F. Bonaccorso, Z. Sun, T. Hasan and A. C. Ferrari, *Nat. Photon.*, 2010, **4**, 611.
11 M. Liu, X. Yin, E. Ulin-Avila, B. Geng, T. Zentgraf, L. Ju, F. Wang and X. Zhang, *Nature*, 2014, **74**, 64.
12 F. Xia, T. Mueller, Y. M. Lin, A. Valdes-Garcia and P. Avouris, *Nat. Nanotechnol.*, 2009, **4**, 839.
13 Q. Bao, H. Zhang, B. Wang, Z. Ni, C. H. Y. X. Lim, Y. Wang, D. Y. Tang and K. P. Loh, *Nat. Photonics*, 2011, **5**, 411.
14 S. Yamashita, *J. Lightwave Technol.*, 2012, **30**, 427.
15 A. Martinez and Z. Sun, *Nat. Photonics*, 2013, **7**, 842.
16 T. Hasan, Z. Sun, F. Wang, F. Bonaccorso, P. H. Tan, A. G. Rozhin and A. C. Ferrari, *Adv. Mater.*, 2009, **21**, 3874.
17 Q. Bao, H. Zhang, Y. Wang, Z. Ni, Y. Yan, Z. X. Shen, K. P. Loh and D. Y. Tang, *Adv. Funct. Mater.*, 2009, **19**, 3077.

18 C. Zaugg, Z. Sun, V. Wittwer, D. Popa, S. Milana, T. Kulmala, R. Sundaram, M. Mangold, O. Sieber and M. Golling, *Opt. Express*, 2013, **21**, 31548.
19 C. Zhao, H. Zhang, X. Qi, Y. Chen, Z. Wang, S. Wen and D. Tang, *Appl. Phys. Lett.*, 2012, **101**, 211106.
20 J. Sotor, G. Sobon and K. M. Abramski, *Opt. Express*, 2014, **22**, 13244.
21 X. Zhang, S. Zhang, C. Chang, Y. Feng, Y. Li, N. Dong, K. Wang, L. Zhong, W. J. Blau and J. Wang, *Nanoscale*, 2015, **7**, 2978; K. Wang, J. Wang, J. Fan, M. Lotya, A. O'Neill, D. Fox, Y. Feng, X. Zhang, B. Jiang and Q. Zhao, *ACS Nano*, 2013, **7**, 9260.
22 Z. Luo, Y. Huang, M. Zhong, Y. Li, J. Wu, B. Xu, H. Xu, Z. Cai, J. Peng and J. Weng, *J. Lightwave Technol.*, 2014, **32**, 4077.
23 S. Lu, L. Miao, Z. Guo, X. Qi, C. Zhao, H. Zhang, S. Wen, D. Tang and D. Fan, *Opt. Express*, 2015, **23**, 11183.
24 I. H. Baek, H. W. Lee, S. Bae, B. H. Hong, Y. H. Ahn, D.-I. Yeom and F. Rotermund, *Appl. Phys. Express*, 2012, **5**, 032701.
25 Z.-C. Luo, M. Liu, H. Liu, X.-W. Zheng, A.-P. Luo, C.-J. Zhao, H. Zhang, S.-C. Wen and W.-C. Xu, *Opt. Lett.*, 2013, **38**, 5212.
26 M. Zhang, E. Kelleher, F. Torrisi, Z. Sun, T. Hasan, D. Popa, F. Wang, A. Ferrari, S. Popov and J. Taylor, *Opt. Express*, 2012, **20**, 25077.
27 N. Tolstik, E. Sorokin and I. T. Sorokina, *Opt. Express*, 2014, **22**, 5564.
28 C. Wei, X. Zhu, F. Wang, Y. Xu, K. Balakrishnan, F. Song, R. A. Norwood and N. Peyghambarian, *Opt. Lett.*, 2013, **38**, 3233.
29 K. F. Mak, C. Lee, J. Hone, J. Shan and T. F. Heinz, *Phys. Rev. Lett.*, 2010, **105**, 136805.
30 J. N. Coleman, M. Lotya, A. O'Neill, S. D. Bergin, P. J. King, U. Khan, K. Young, A. Gaucher, S. De and R. J. Smith, *Science*, 2011, **331**, 568.
31 W. S. Yun, S. W. Han, S. C. Hong, I. G. Kim and J. D. Lee, *Phys. Rev. B: Condens. Matter*, 2012, **85**, 033305.
32 J. Wilson and A. Yoffe, *Adv. Phys.*, 1969, **18**, 193.
33 H. Zhang, S. Virally, Q. Bao, K. P. Loh, S. Massar, N. Godbout and P. Kockaert, *Opt. Lett.*, 2012, **37**, 1856.
34 H. Shi, R. Yan, S. Bertolazzi, J. Brivio, B. Gao, A. Kis, D. Jena, H. G. Xing and L. Huang, *ACS Nano*, 2013, **7**, 1072.
35 B. Xu, P. Camy, J.-L. Doualan, Z. Cai and R. Moncorgé, *Opt. Express*, 2011, **19**, 1191.